Response of a colloidal gel to a microscopic oscillatory strain

Myung Han Lee and Eric M. Furst*
Department of Chemical Engineering, University of Delaware, Colburn Laboratory, 150 Academy Street, Newark, Delaware 19716, USA
(Received 15 August 2007; published 22 April 2008)

We study the microscopic mechanical response of colloidal gels by manipulating single probe particles within the network. For this work, we use a refractive index and density-matched suspension of polymethylmethacrylate (PMMA) particles with nonadsorbing polymer: polystyrene. As the polymer concentration increases, a dynamically arrested, space-filling network is formed, exhibiting structural transitions from a clusterlike to a more homogeneous stringlike gel phase, consistent with observations by Dibble and co-workers [C. J. Dibble, M. Kogan, and M. J. Solomon, Phys. Rev. E **74**, 041403 (2006)]. In a gel, probe particles are oscillated with an optical trap, creating the local strain field in the network. We find that the micromechanics correlate strongly with the gel structure. At high polymer concentration, the average deformation field decays as $1/r$ to a distance quite close to the probe particle, as expected for a purely elastic material. In contrast, at lower polymer concentrations, gels exhibit anomalous strain fields in the near field; the strain plateaus, indicating that many particles move together with the probe. By rescaling the probe size in the theoretical model, we obtain a micromechanical gel correlation length, which is consistent with the structural difference in terms of "clusterlike" and "stringlike."

DOI: 10.1103/PhysRevE.77.041408 PACS number(s): 82.70.Gg, 82.70.Dd, 62.20.Hg

I. INTRODUCTION

Colloidal gels display a number of important rheological properties, such as yield stress and elasticity [1–3]. The control of their properties is essential to many technological applications, such as the processing of ceramics, coatings, inks, and numerous foods. This need represents one of the most important challenges to our understanding of colloidal gels. The rheological properties of gels can be tuned by adjusting the strength and range of interparticle attractions and the particle volume fraction [4–6]. In particular, the strong dependence of rheological behavior on particle volume fraction implies that the connectedness and topology of the gel microstructure considerably affect the elastic deformation and yielding of gels. Therefore, a better understanding and controlling of the rheology of colloidal gels results from characterizing the microstructure and its corresponding mechanical response. Clearly, such an understanding will ultimately lead to more accurate predictions and better control of process and final material properties.

The relationship between the structure and rheology of gels has been extensively studied [7–16]. For colloidal gels at low particle volume fractions, the dependence of the rheological behavior on the microstructure is well described by scaling models based on the fractal description of the network [7–11]. With sufficiently strong attractive interactions, dispersed colloidal particles form aggregates of N particles with the cluster size $\xi \approx aN^{1/D_f}$, where D_f is the fractal dimension and a is the particle radius [17,18]. The growth proceeds until the clusters span the whole system, ultimately forming a dynamically arrested gel. The rheology of such fractal gels has been modeled based on the underlying microstructure mechanics [7–11], as suggested by Kantor and Webman [19]. The elastic modulus and yield stress scale as $G' \sim \phi^{(3+x)/(3-D_f)}$ [9] and $\sigma_y \sim \phi^{2/(3-D_f)}$ [10], respectively, where x is the bond dimension. Similar expressions, also based on the fractal description of a structure, have been found to capture the power-law behavior with respect to particle volume fraction and agree well with experimental measurements [8,12].

In contrast, for colloidal gels at higher particle volume fractions, the fractal description of microstructure is no longer suitable [20–22]. In this regime, a gel network can exhibit various degrees of arrest and densification, depending on the particle volume fraction and the nature and magnitude of the attractive forces [23–25]. This has a significant influence on the mechanical and rheological properties of colloidal gels [13–16]. For instance, Channell and co-workers examined the effect of gel microstructure on the compressive yield stress for flocculated alumina suspensions ($0.25 \leq \phi \leq 0.50$) using a centrifugation technique [14]. They found that the presence of heterogeneities such as large voids and dense, nonfractal clusters in a gel reduces the compressive yield stress, apparently since individual dense clusters were connected by weak bonds to form a space-filling network. In contrast, Wyss and co-workers studied the mechanical behavior of concentrated silica gels with significantly different microstructures [13]. They reported an increase of elasticity and yield stress with increasing heterogeneity of the gel microstructure, since they form a bicontinuous network.

Recent theoretical work has also addressed the effect of structural heterogeneity on the mechanical properties of colloidal gels beyond the fractal regime [1,15,16]. In comparisons of mode-coupling theory (MCT) in conjunction with the polymer reference interaction site model (PRISM) to experiments, the theoretical calculations of the elastic modulus G'_{MCT} are ~ 100 times larger. This discrepancy has been explained by the presence of heterogeneities on the length scale of a few particle diameters, observed by ultrasmall-angle x-ray scattering measurements [1]. As a consequence, they have suggested a numerical prefactor correction of G'_{MCT} to account for this effect based on the fact that dense clusters,

*Corresponding author. furst@udel.edu

not single particles, transmit the stress. The corrected modulus $G' = G'_{\mathrm{MCT}}/N_c$ accounts for the number of particles per cluster of radius ξ_c, where ϕ_{cluster} is the particle volume fraction in a cluster, and thus, $N_c \approx \phi_{\mathrm{cluster}}(\xi_c/a)^3$. The values of ξ_c necessary to achieve quantitative agreement between theory and experiment are consistent with the scattering experiments and typically lie in the range of $\xi_c/2a \sim 3-4$.

The fundamental relation between a local structure and rheology in nonfractal gels has yet to be completely understood. This is partly attributed to the difficulties involved in characterizing the microstructure and its response to perturbation in a dense gel. In this paper, we study the microscopic response of colloidal gels to a microscopic oscillatory strain using the combined techniques of optical tweezers and confocal microscopy. The dynamics and microstructure in a similar system have been studied by Dibble and co-workers [26]. In their studies, a sequence of fluid, fluid cluster, immobile cluster, and gel phases were observed with gradually increasing polymer concentration. They identified mobile (i.e., fluid and fluid cluster) and immobile phases (i.e., immobile clusters and gels) by observing an abrupt decrease of the suspension dynamics. Furthermore, they found that the transition from an immobile cluster to gel phases leads to a decrease of structural heterogeneity; in the immobile cluster phase, long-range structural heterogeneity on a characteristic length scale beyond ~30 colloid radii was found, while in the gel phase, a more homogeneous, stringlike structure on the length scale of ~10 colloid radii was observed. Our studies confirm these key observations of structural and dynamical transitions, while providing new information about their correlation to the microscopic mechanical behavior of gels.

We begin with an overview of materials and methods, including details of the sample preparation, experimental techniques, and particle tracking. In Sec. III A, we characterize the dynamics and microstructure of the suspensions by varying the polymer concentration. We quantify the dynamics, allowing us to identify the transition to the immobile or arrested phase. Structurally, we investigate the average bond number and number density fluctuation of the immobile phases. In Sec. III B, we report measurements of the strain fields induced by the oscillating motion of an optically trapped probe. Specifically, we study the spatial range of this perturbation and distance dependence of the deformation fields, including how they vary with the amplitude of the probe oscillation and polymer concentration. Finally, we compare the measured strain fields with the theoretical calculations for a purely elastic material and detail the effect of structural heterogeneity on the strain fields. We summarize the main points of this work in Sec. IV.

II. EXPERIMENT

A. Sample preparation

Experiments are performed using poly(12-hydroxystearic acid) (PHSA) stabilized poly(methyl methacrylate) (PMMA) spheres fluorescently labeled with nile red (excitation wavelength $\lambda_{ex}=548$ nm, emission wavelength $\lambda_{em}=567$ nm). The PMMA particles, with mean diameter $2a=1.53$ μm (polydispersity=5.79%), are dispersed in a refractive index and density-matched solvent composed of a mixture of decalin and cyclohexyl bromide (CHB). A short-range attraction is induced by the addition of a nonadsorbing polymer, polystyrene (Pressure Chemical Co., $M_w=900\,000$, $M_w/M_n=1.06$) with radius of gyration $R_g=41\pm4$ nm [26], overlap concentration $C_P^*=5.3$ mg/ml, and $\Delta=R_g/a=0.054$. In this work, the polymer concentration is varied from 1.0 to 13.4 mg/ml at a constant particle volume fraction $\phi=0.20$. Polymer concentration C_p is defined as the mass of polymer divided by the volume of solvent, $V(1-\phi)$, where V is the total volume of solution. We note that reported C_p values are nominal concentrations. In the semidilute regime which is above the overlap concentration, the polymer is characterized by the correlation length $\xi_p=R_g(C_p/C_p^*)^{-0.75}$ [27,28], rather than R_g, which is 26 nm and 20 nm for $C_p=10.0$ and 13.4 mg/ml, respectively. The depletion potential range is $\xi_{\mathrm{dp}}=2R_g$ for the dilute polymer regime and $\pi\xi_p$ for the semidilute regime [29,30].

We note that the polymer solutions do not contribute significantly to the elastic response by measuring the viscoelastic properties of polymer solutions over the frequency in the range of 30–1200 rad/s using an oscillating trap (data not shown) [31,32]. For all polymer concentrations used, the elastic modulus of the polymer solutions is below our measurement threshold. In addition, the viscosity of polymer solutions exhibits common behavior with a slight increase in the dilute regime and a steep increase at higher concentration ($>C_p^*$) (data not shown).

In the PMMA gel, a small number of melamine microspheres ($2a_p=2.0$ μm, $\phi_p<10^{-3}$) are added as probe particles. Melamine particles have a refractive index of $n_p=1.68$, which provides sufficient, but not excessive mismatch to the colloid-polymer dispersion, $n\sim1.49$. This enables the index-mismatched melamine particles to be optically trapped. There is a slight density difference between melamine ($\rho_p=1.51$ g/cm^3) and the PMMA gel ($\rho=1.18$ g/cm^3); however, the heavier melamine particles are strongly attracted to the PMMA gel network [33], which prevents their sedimentation. Melamine particles do not significantly swell in mixtures of decalin and CHB, which is determined by monitoring the probe size over time.

Samples are prepared by mixing four stock liquids: (I) a 40 vol % PMMA dispersion in decalin/CHB, (II) a 30 mg/ml polystyrene solution in decalin/CHB, (III) a 0.2 vol % melamine dispersion in decalin/CHB, and (IV) decalin/CHB. Each of these stock solutions is prepared by adding PMMA, polystyrene, or melamine to a mixture of 34.4 vol % decalin and 65.6 vol % CHB, and dispersing them using a vortex mixer (1 min) followed by bath sonication (30 min). These solutions are quiescently equilibrated for 10 h. Next, the four solutions are mixed together using a vortex mixer for 1 min. By centrifugation (10 min and 10 000 rpm), we ensure a density matching of particles. If the particles settle, we add a small amount of CHB. Likewise, if particles rise, we add a small amount of decalin. The density-matching process is then repeated. After density matching, samples are redispersed using a bath sonicator (3 min) and vortex mixer (1 min). The refractive index does not change significantly over these slight variations in solvent composition, due to the similar refractive indexes of the two solvents (n_{decalin}

$=1.47$, $n_{CHB}=1.50$). Under density-matching conditions, the refractive index of the binary liquid mixture is approximately 1.49, as determined by the Lorentz-Lorenz equation

$$\frac{n_{12}^2-1}{n_{12}^2+2}=\phi_1\frac{n_1^2-1}{n_1^2+2}+\phi_2\frac{n_2^2-1}{n_2^2+2}, \quad (1)$$

where n_{12} is the refractive index of the solvent mixture, and n_i and ϕ_i are index and volume fraction of the pure components, respectively. The solvent mixture is nearly refractive index matched with the PMMA particles ($n=1.49$), ensuring that the PMMA particles are not optically trapped.

Following this preparation, we introduce the suspension into sample cells composed of a No. 1 cover glass, glass microscope slide, and a 0.2-mm gap constructed with glass spacers. All parts are held by a uv cure epoxy (Norland products NOA 81). The sample area is approximately 10 mm $\times 20$ mm. A sample is injected into the cell via capillary action and carefully sealed with epoxy for 5 min to prevent drying of the solvent and photobleaching of the fluorescent particles. Samples are equilibrated before use for 3 h.

B. Optical tweezers and confocal microscopy

We use a combination of optical tweezers and confocal microscopy to induce and characterize a local perturbation. Laser tweezers are used to manipulate single probe particles embedded in the gel network. To generate the traps, a single beam with transverse mode TEM_{00} from the 1064-nm line of a 4-W Nd:YAG laser is introduced into the side port of an inverted microscope (Zeiss Axiovert 200). The beam is expanded to overfill the back aperture of a 1.4-numerical-aperture $100\times$ oil-immersion objective (Zeiss Planapochromat), which results in highly focused light in our sample. The trap position in the focal plane of the microscope is controlled using an acousto-optic deflector (AA Opto-electronics, AA.DTS.XY-400). The intensity of the trap beam at the back aperture of the objective is approximately 320 mW, corresponding to a trap stiffness in the range of $k_t=10-12$ pN/μm. The maximum trapping force is 8.2 ± 0.5 pN, determined by the maximum viscous drag force on the melamine particles [33].

The gel microstructure is imaged with a Nipkow confocal microscope (Yokogawa Electric Co., Model CSU10) [34]. Images are captured using a 10-bit intensified charge-coupled-device (CCD) camera (Stanford Photonics XR-MEGA/10) and stored on a hard drive for later processing. Three-dimensional (3D) image volumes can be obtained under quiescent conditions. These are reconstructed by collecting 2D image slices using a piezo-objective positioner (Physik Instrumente, Model P-721.CDQ).

Three-dimensional image processing is carried out on the image volumes to generate the 3D particle positions, using a modified version of the 2D particle-tracking algorithms described by Crocker and Grier [35]. This procedure includes the spatial bandpass filtering of the images and location of 3D particle centers within a half a voxel determined as the voxel of the locally brightest intensity in a particle volume. The position of each center is then refined to the subvoxel accuracy by way of moments of the local intensity distribution. We estimate that the image acquisition error of the particle positions is less than 30 nm in the x-y direction and 40 nm in the z direction.

Next, the colloidal gel response to oscillatory motion of a trapped probe is measured in more than seven different locations for each sample. Melamine probe particles dispersed in the PMMA-PS gel are oscillated for 5–6 periods with the optical trap at a constant frequency of 0.02 Hz and laser amplitudes of 0.55 and 1.09 μm, which induces a local perturbation of the network. Confocal imaging enables simultaneous observations of the gel response to this microscopic perturbation. Confocal images are captured at 18 frames per second, and 16 frames are averaged to reduce noise and improve particle tracking. The low oscillation frequency ensures that hydrodynamic interactions do not play a role in the microscopic response.

C. Particle tracking

We analyze confocal images to quantify the response of gel particles under the imposed strain as following: The 2D image-processing methods of Crocker and Grier [35] are used to locate the gel particles in individual image frames and subsequently generate trajectories. Then, the particle trajectories are analyzed for in-phase motion with the oscillating probe particle by taking the discrete Fourier transform (DFT) [36]

$$F(\nu_f)=N^{-1}\sum_{\tau=0}^{N-1}f(\tau)e^{-i2\pi(\nu_f/N)\tau}, \quad (2)$$

where N is total number of discrete samples taken and ν_f/N is analogous to the frequency measured in cycles per sampling interval. This is critical for distinguishing the small motion induced by the probe particle from localized thermal fluctuations in the gel. The power spectrum of particles in the gel moving in phase with the forced probe motion exhibits a maximum at the probe oscillation frequency, as shown in Fig. 1. Equation (2) is defined such that the magnitude of a maximum peak in the frequency domain corresponds to half of the particle's real-space amplitude. Each particle can then be assigned an amplitude corresponding to its response to the probe.

The direction of gel particle displacement is given by $\theta=P\tan^{-1}(|\vec{u}_y|/|\vec{u}_x|)$, where $|\vec{u}_x|$ and $|\vec{u}_y|$ are the particle's amplitudes in the x and y directions, determined by discrete Fourier transform, and P is a directional factor for strain along the y direction. During the half cycle where the probe particle moves from left to right, if the gel particle moves upwards, $P=1$, while if the particle moves down, $P=-1$. Note that the oscillation frequency of 0.02 Hz is low to prevent significant phase lag between the gel particles and the probe [32].

III. RESULTS AND DISCUSSION

A. Dynamics and microstructure

First, we examine the dynamics of the suspensions as a function of polymer concentration to identify the transition to immobile phases (i.e., immobile clusters or gels), which

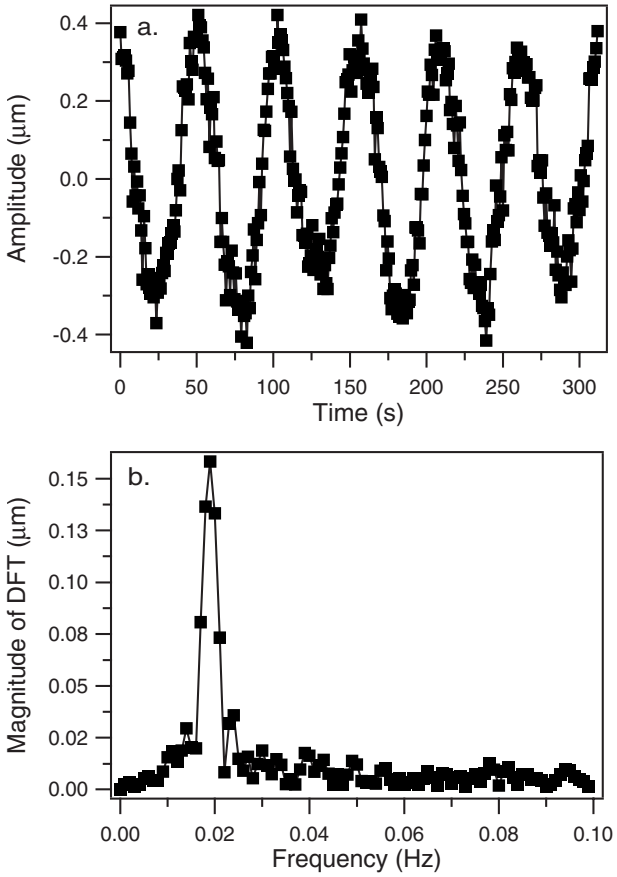

FIG. 1. (a) x-axis projection of a particle trajectory which is in phase with the probe motion. (b) The frequency spectrum from discrete Fourier transform (DFT) of a particle x trajectory.

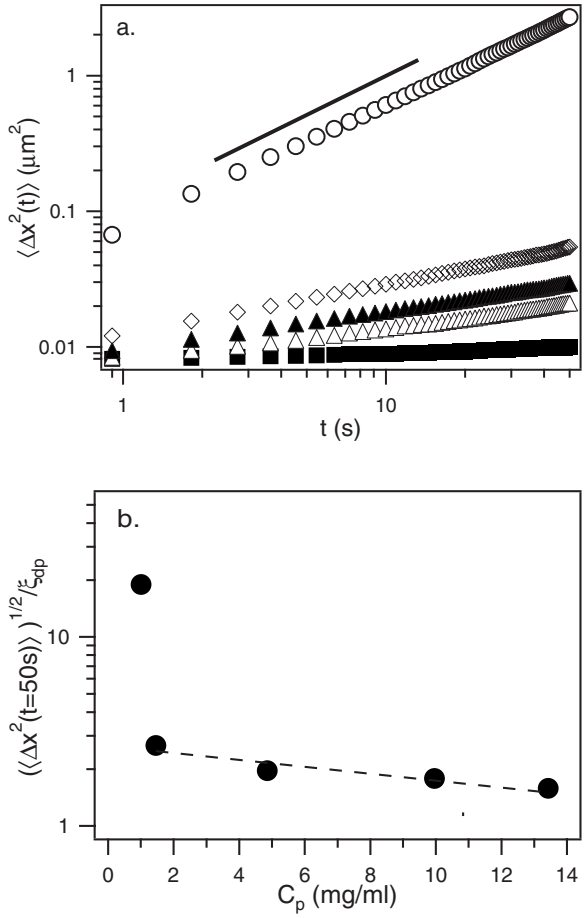

FIG. 2. (a) Mean-squared displacement as a function of nonadsorbing polymer concentration C_p: (◯) C_p=1.0 mg/ml, (◇) C_p=1.5 mg/ml, (▲) C_p=4.9 mg/ml, (△) C_p=10.0 mg/ml, and (■) C_p=13.4 mg/ml. (b) Square root of the mean-squared displacement normalized to the depletion potential range, $\sqrt{\langle \Delta r^2(t=50\ \mathrm{s})\rangle}/\xi_{\mathrm{dp}}$, as a function of C_p.

are dynamically arrested. We note that similar results with respect to these physical characteristics have been described previously [26]. However, our purpose here is twofold: to provide context for the micromechanical results and to verify the observations of Dibble and co-workers for the particular system investigated in this study. Figure 2 shows the behavior of single-particle mean-squared displacement with increasing polymer concentration. At C_p=1.0 mg/ml, the mean-squared displacement is similar to self-diffusion, $\langle \Delta x^2(t)\rangle \sim t$, corresponding to a fluid. As the polymer concentration increases, the dynamics slow and exhibit increasing subdiffusion. At the highest polymer concentration (13.4 mg/ml), the mean-squared displacement is independent of time. The transition from a mobile cluster phase to the immobile phases is characterized through the localization length $\sqrt{\langle \Delta x^2(t=50\ \mathrm{s})\rangle}/\xi_{\mathrm{dp}}$, which is estimated from the mean-squared displacement of PMMA particles. The localization length decreases significantly between C_p=1.0 and 1.5 mg/ml, indicating the dynamics transition to highly localized behavior. This corresponds to a highly arrested, space-filling network, known as "immobile phases" [26]. A further increase in the polymer concentration leads to a decrease of the localization length to approximately ξ_{dp}—that is, comparable to the range of the depletion potential.

Next, we characterize the microstructure as a function of increasing polymer concentration at ϕ=0.20. Figure 3 shows confocal images at four polymer concentrations (C_p=2.0, 5.1, 10.0, and 13.4 mg/ml), which are selected in the immobile phases. At the lowest polymer concentration (C_p=2.0 mg/ml), the structure is denser than others. As the polymer concentration increases to C_p=5.1 and 10.0 mg/ml, the structure consists of locally dense clusters and open voids, reminiscent of an arrested spinodal decomposition [37]. In contrast, at the highest polymer concentration (C_p=13.4 mg/ml), gels exhibit a more homogeneous structure. The qualitative observations of structure are quantified below by calculating the average bond number and number density fluctuations for each case.

To characterize the structure of the gels on short length scales, we determine the average number of nearest neighbors in contact, or bond number N_b, for each particle. Two particles are considered to be in contact when the distance between centers is less than the sum of the particle diameter and the range of depletion potential, $2a+\xi_{\mathrm{dp}}$. Figure 4 shows the average bond number N_b as a function of C_p for ϕ=0.20. The average bond number at the lowest polymer concentration (2.0 mg/ml) is greater than those at higher concentrations C_p ($\geq$5.1 mg/ml). Above 5.1 mg/ml, the average

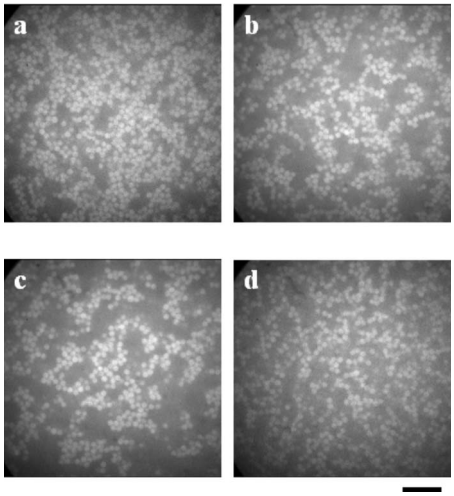

FIG. 3. Confocal images of the structure formed at $\phi=0.20$ as a function of C_P: (a) 2.0 mg/ml, (b) 5.1 mg/ml, (c) 10.0 mg/ml, and (d) 13.4 mg/ml. Confocal images are captured 3 h after preparing the samples. The scale bar is 10 μm.

bond number does not change significantly; the average value is 2.9.

The number density fluctuation $(\langle N^2\rangle-\langle N\rangle^2)/\langle N\rangle$ provides a useful means for evaluating the structure on long length scales [38,39]. The density fluctuations are calculated by dividing 3D confocal images into smaller subvolumes of dimension L and counting the number of particles in each subvolume. In the limit $1/L\rightarrow 0$, the number density fluctuation is related to the low scattering vector limit of the structure factor and the gel isothermal compressibility χ_T [38,40]:

$$S(q\rightarrow 0)=\lim_{a/L\rightarrow 0}\frac{\langle N^2\rangle-\langle N\rangle^2}{\langle N\rangle}=\rho k_B T\chi_T. \tag{3}$$

In our study, L is limited to 10 μm by the smallest dimension of the confocal volume ($40\times 40\times 10$ μm^3), corresponding to $a/L=0.8$.

Figure 5 shows the number density fluctuations with increasing polymer concentration. At polymer concentrations below 10.0 mg/ml, the density fluctuations increase with increasing L, indicating the presence of significant heterogeneity in the network. However, unlike previous studies [26], we could not identify a maximum peak corresponding to a characteristic length scale. This might be due to the broad size distribution of clusters, some of which span beyond the longest observed length scale. Nonetheless, at $C_p=13.4$ mg/ml, the density fluctuations exhibit starkly different behavior, decreasing with increasing L. This corresponds to a more homogeneous distribution of particles throughout the volume. Thus, the structure is divided into a clusterlike phase (again, suggestive of an arrested spinodal decomposition) below 10.0 mg/ml and stringlike and more homogeneous gel at the relatively high polymer concentration, 13.4 mg/ml. The structural transitions based on the polymer concentration we observed are consistent with previous studies in a similar system reported by Dibble and co-workers [26].

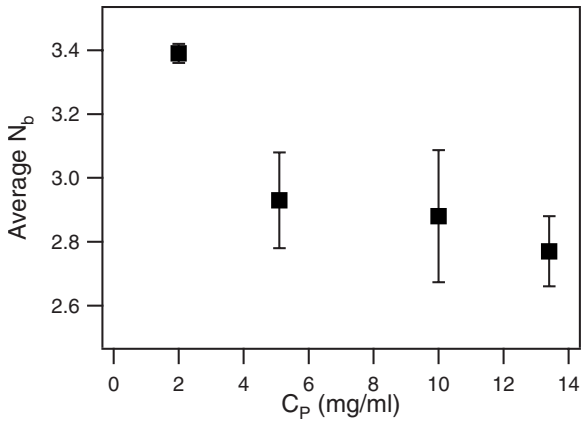

FIG. 4. Average bond number at $\phi=0.20$ with increasing C_P.

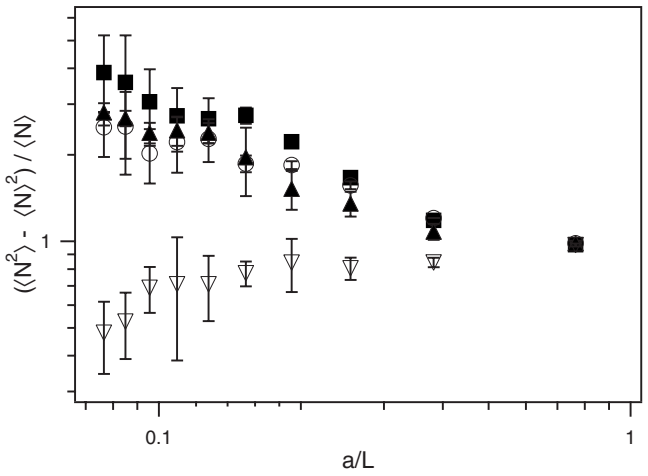

FIG. 5. Number density fluctuation $(\langle N^2\rangle-\langle N\rangle^2)/\langle N\rangle$ as a function of subvolume size L for $\phi=0.20$: (■) $C_p=2.0$ mg/ml, (◯) $C_p=5.1$ mg/ml (▲) $C_p=10.0$ mg/ml, and (▽) $C_P=13.4$ mg/ml.

B. Strain fields induced by probe oscillation

In this work, probe particles are introduced and manipulated with optical traps. These probe particles belong to the gel network. A single probe particle oscillation creates local strain fields in a gel network, as shown in Fig. 6. In this figure, dots indicate tracked particles which exhibit purely Brownian motion and negligible movement in phase with the probe. More precisely, the power spectrum of particle trajectories does not exhibit a maximum at the probe oscillation frequency of 0.02 Hz, as we discussed in Sec. II C. For the particles that move in phase with the probe, the arrows indicate the direction of the local strain for half the oscillation period, while the color scale shows the amplitude of the displacements. The magnitude and direction of the gel particle displacement strongly depends on its location (i.e., the distance from the probe). As expected, the magnitude of the displacement decreases with increasing distance from the probe. For the field direction, in the near field, particles mainly move at the same direction as probe motion, while in the far field, they exhibit random motion.

The most striking feature of the strain induced in the gel, however, is the length scale over which the perturbation extends. Notably, it is strongly and nonmonotonically depen-

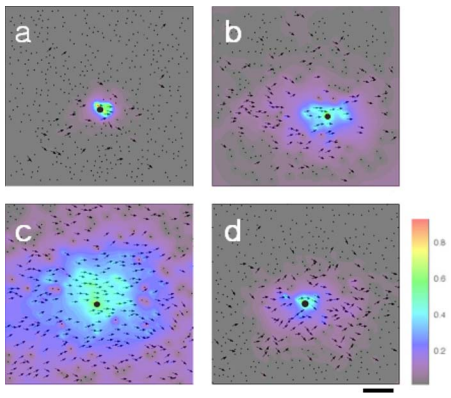

FIG. 6. (Color online) Local strain fields induced by probe oscillation with the laser amplitude of 1.09 μm as a function of C_P: (a) 2.0 mg/ml, (b) 5.1 mg/ml, (c) 10.0 mg/ml, and (d) 13.4 mg/ml. The color bar indicates the amplitude of particle with units of micrometers. The probe particle is oscillated left to right. The black circle represents the size and location of the probe.

dent on the polymer concentration. At the lowest polymer concentration C_p=2.0 mg/ml, the perturbation is highly localized near the probe particle. In the case shown, only a half dozen particles within 3 μm of the probe move significantly. At this polymer concentration, a dynamically arrested, gellike structure is formed, as discussed before. However, the interparticle potential is relatively weak, resulting in a fragile microstructure incapable of maintaining the network even under small perturbations. The strain induced by the probe is not transmitted continuously along the gel network due to bond ruptures and rearrangements. As C_p increases, however, the bond strength is sufficient to produce long-range deformation of the gel network. Interestingly, as the perturbation length increases, it reaches a maximum at 10.0 mg/ml and then decreases at the highest polymer concentration of 13.4 mg/ml.

Figure 7 shows average strain fields of gels averaged from more than seven different locations in each sample. The

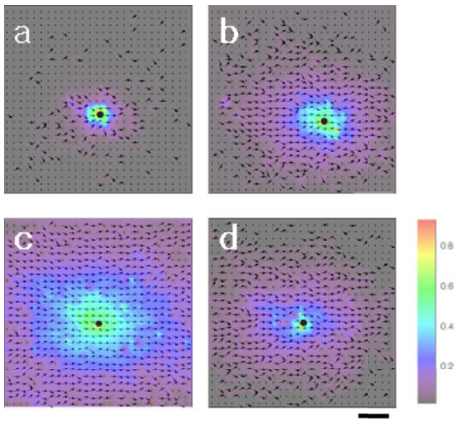

FIG. 7. (Color online) Average strain fields induced by probe oscillation with the laser amplitude of 1.09 μm as a function of C_P: (a) 2.0 mg/ml, (b) 5.1 mg/ml, (c) 10.0 mg/ml, and (d) 13.4 mg/ml. The color bar indicates the amplitude of displacement with units of micrometers. The probe particle is oscillated left to right. The black circle represents the size and location of the probe.

trends of the average strain are similar to those discussed for Fig. 6. First, the length scale of strain propagation is nonmonotonic with polymer concentration. The lowest polymer concentration shows a considerably weak, if any, propagation of strain. At C_p=10.0 mg/ml, the perturbation length reaches a maximum. It then decreases at the highest polymer concentration of 13.4 mg/ml. In the near field, the average strain is parallel to the probe motion and particle displacement in the gel perpendicular to the probe motion is relatively small, as we discuss in reference to Eqs. (5) and (6) below.

Before quantitatively examining the strain propagation in the gels, we first consider the deformation field $\vec{u}(\vec{x})$ due to an embedded particle with a displacement vector $\vec{U}$ in a purely elastic medium:

$$\vec{u}(\vec{x}) = \frac{3a}{10-12\nu}\left[\left(\frac{3-4\nu}{r}+\frac{a^2}{3r^3}\right)\vec{U}+\left(1-\frac{a^2}{r^2}\right)\frac{\vec{U}\cdot\vec{x}\vec{x}}{r^3}\right], \tag{4}$$

where ν is the Poisson ratio and $\vec{x}$ is the particle position [41]. Assuming ν=1/2, the displacements in the x and y directions are given by

$$|\vec{u}_x(r,\theta)| = \frac{3a}{10-12\nu}\left[\left(\frac{3-4\nu}{r}+\frac{a^2}{3r^3}\right)U_x + \left(1-\frac{a^2}{r^2}\right)\frac{1}{r^3}U_x(r\cos\theta)^2\right] \tag{5}$$

and

$$|\vec{u}_y(r,\theta)| = \frac{3a}{10-12\nu}\left[\left(1-\frac{a^2}{r^2}\right)\frac{1}{r^3}U_x r^2\cos\theta\sin\theta\right], \tag{6}$$

respectively. Theoretical strain fields for the both x and y components are calculated from Eqs. (5) and (6). To the leading order, they decrease from the probe particle as $1/r$ and the magnitude of strain fields in the x direction is one order of magnitude higher than that in the y direction (data not shown).

Next, note that the magnitude of the probe displacement, U_x, is a function of polymer concentration due to changes in the mechanical properties of the network. Consider the response of a probe particle in an oscillating optical trap with a displacement described by $A\cos(\omega t)$, where A is the amplitude of trap and ω is its angular frequency. The response function of the probe particle is given by

$$x_p(t) = U_x(\omega)\cos[\omega t - \delta(\omega)], \tag{7}$$

where the particle amplitude and the phase shift are

$$U_x(\omega) = \frac{Ak_t}{\sqrt{(k_t+k_e)^2+(6\pi a\eta\omega)^2}} \tag{8}$$

and

$$\delta(\omega) = \tan^{-1}\left(\frac{6\pi a\eta\omega}{k_t+k_e}\right), \tag{9}$$

respectively [32]. In Eqs. (8) and (9), k_e is the effective elasticity and η is the viscosity of the surrounding material. As

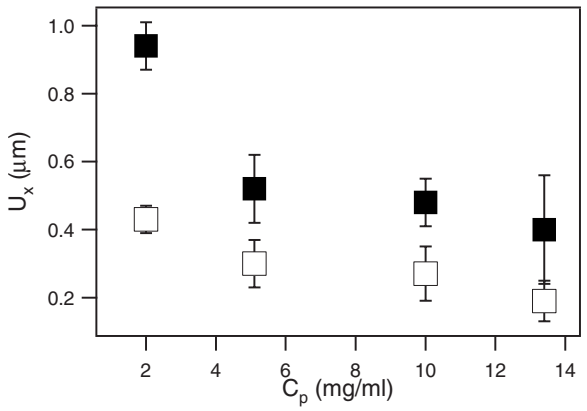

FIG. 8. Probe displacement vector magnitude U_x as a function of polymer concentration C_P. The symbols are measurements made at the laser amplitude of (□) 0.55 μm and (■) 1.09 μm.

the attractive forces between particles increase, the elastic constant k_e increases, leading to a decrease in the particle amplitude U_x at the same frequency. In our experiments, the magnitude of the probe particle displacement is determined for each probe by measuring the amplitude of the nearest PMMA particle neighbors in contact, as shown in Fig. 8. As C_p increases, the probe displacement decreases, reflecting an increase in the local stiffness of the gel. In particular, the probe displacement decreases significantly between C_p=2.0 and 5.1 mg/ml, while above C_p=5.1 mg/ml, it decreases only slightly more. For the same samples, the probe displacement magnitude at a laser amplitude of 1.09 μm is greater than that at a laser amplitude of 0.55 μm, as expected.

The average deformation in the gel for all polymer concentrations and the corresponding theoretical calculations using U_x are shown in Fig. 9 for two strain amplitudes. The orange (light gray) lines represent the expected response for a purely elastic material [Eq. (5)] at low (dashed line) and high (solid line) strains. Note that we correct for the angular dependence of the strain field by plotting $\langle |U_x|/(1+\cos^2\theta)\rangle$ and $\langle |U_y|/|\cos\theta \sin\theta|\rangle$ versus r/a. In all cases except for the lowest polymer concentration, 2.0 mg/ml, the far-field x component of the strain scales as $1/r$, as expected for an elastic solid. In contrast, for C_p=2.0 mg/ml, the displacement decreases discontinuously, probably due to the extreme fragility of the structure with such weak attractions. Surprisingly, for C_p=13.4 mg/ml, this scaling behavior continues down to distances quite close to the probe particle. For C_p =5.1 and 10.0 mg/ml, however, the strain plateaus in the near field, indicating that the particles are moving with the probe a greater amount than expected; that is, their movement is more akin to a rigid body than an elastic medium.

To account for the near-field behavior, we rescale the probe size in Eq. (5) for the all cases except for C_p =2.0 mg/ml, as shown in Fig. 10, to fit the far-field deformation of the gel. In Fig. 9, the revised strain fields are shown as red (dark gray) lines based on this new effective probe size a_p^{eff}. At C_p=5.1 and 10.0 mg/ml, we find that, on average, the gel moves as a rigid body in an elastic medium

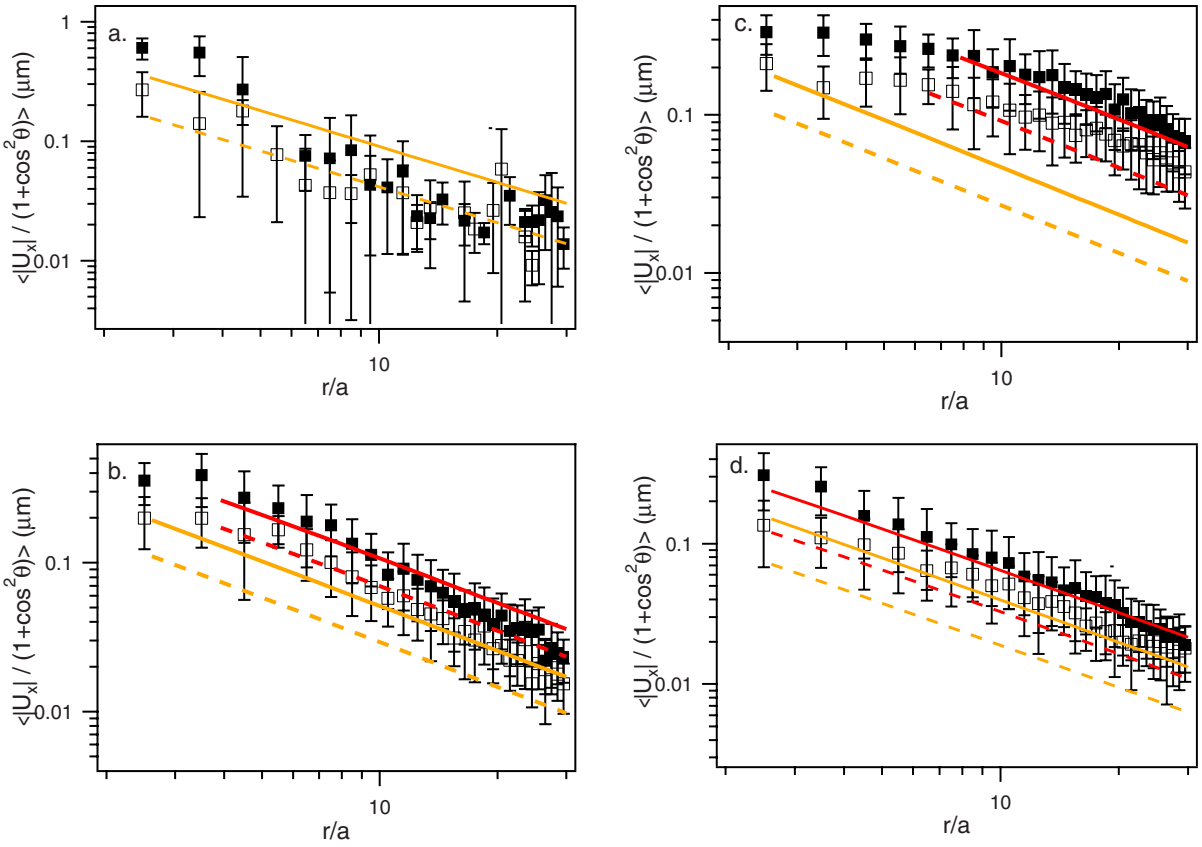

FIG. 9. (Color online) The projected strain fields for the gel surrounding an oscillating probe particle as a function of C_P: (a) 2.0 mg/ml, (b) 5.1 mg/ml, (c) 10.0 mg/ml, and (d) 13.4 mg/ml.

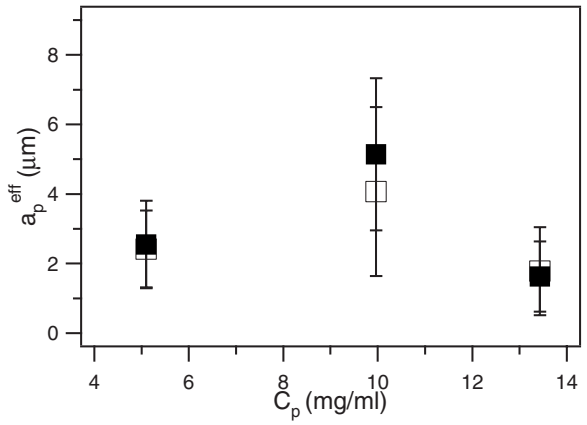

FIG. 10. Effective probe size a_p^{eff} with increasing polymer concentration C_P. The symbols are measurements made at the laser amplitudes of (□) 0.55 μm and (■) 1.09 μm.

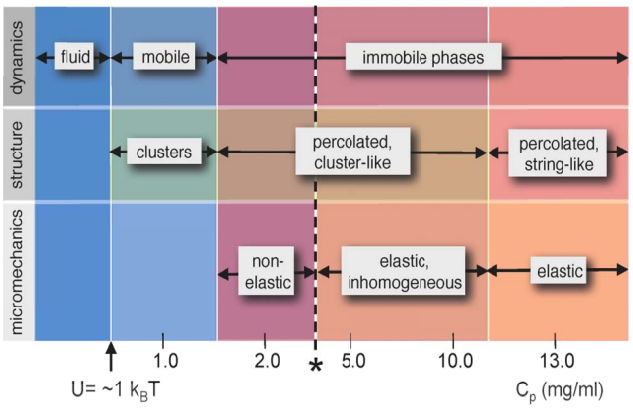

FIG. 11. (Color online) Summary of correlations between dynamics, microstructure, and micromechanics of depletion gels for ϕ=0.20 as the depletant polymer concentration increases. The asterisk denotes the region of transition from nonelastic behavior to an elastic gel.

with an effective radius of 2.6 and 5.1 μm, respectively. At C_p=13.4 mg/ml, a_p^{eff} decreases to 1.6 μm, very close to the actual probe radius. Consequently, these micromechanics provide an estimate for a new micromechanical correlation length in the gels, which correlates with the transition from "clusterlike" to "stringlike" structures captured by the number density fluctuations. It is important to note that trappable probe particles incorporated in the gel network do not appear to alter the local structure around the probes. To test this, we calculate the 2D average bond numbers with increasing radial distance from both the probes and gel particles, respectively (data not shown). The topology and average bond numbers around probes are the same as those at other points in the gel.

Two significant concluding observations can be made from these micromechanical studies. First, the emergence and nonmonotonic nature of the mechanical length scale characterized by the near-field deformation plateau in Fig. 9 may have important rheological consequences, particularly for the compressive yield stress, shear yield stress, and modulus of gels. As mentioned above, recently, the effect of structural heterogeneity on the mechanical properties of colloidal gels has been studied by Schweizer and co-workers using the MCT-PRISM [1,15,16]. They found that large quantitative differences between MCT-PRISM predictions of elastic moduli and experiments are due to the formation of nonequilibrium dense clusters in the gel. Correcting for the structural heterogeneity led to quantitative agreement between theoretical calculations and measurements. In such cases, the elementary mechanical unit is not a single colloid, but a small, dense cluster in the networks. The micromechanics investigated here suggest that the gel network modulus will be nonmonotonic with polymer concentration between 2 mg/ml and 13 mg/ml. Such mechanics could play an important role in delayed sedimentation.

Second, the experiments provide a refined view of the point at which the properties of attractive colloidal systems constitute a gel based on the relationships between the dynamics, structure, and micromechanics. These relationships are summarized in Fig. 11. In this study, the initial transition from mobile clusters to percolated and dynamically arrested clusters occurs at 2 mg/ml of depletant polymer. As noted earlier, this structure is quite dense, and exhibits a maximum in the average bond number per particle (cf. Figure 4). However, despite having nearly identical structural and dynamic properties as gels formed at higher polymer concentrations, the microrheology is fluidlike and the microstructure does not propagate deformation as an elastic solid. Only after the bond number decreases from this maximum value of 3.4 to a nearly constant value of 2.8 at polymer concentrations above 5 mg/ml does the microstructure exhibit significant elastic properties. Thus, the transition to a gel capable of transmitting stress elastically is a subtle one, but can be identified by a combination of the structural, dynamical, and micromechanical properties. We note that the line drawn in Fig. 11 demarcating the distinction between the elastic and nonelastic behavior should not be taken as a precise concentration based on our results, but instead lies within the narrow range of polymer concentrations between 2 and 5 mg/ml. The other structural transition occurring within the elastic gel phase is the transition from clusterlike to more stringlike arrangements. This is clearly correlated with a transition from "inhomogeneous" elastic properties to structures that, on average, propagate microscopic deformations similar to a homogeneous elastic solid.

IV. CONCLUSIONS

In this work, we provided insight into the microstructure response of a depletion gel, using simultaneous confocal microscopy and optical tweezer measurements. First, we investigated the dynamics and structure of depletion gels with increasing polymer concentration at ϕ=0.20. Through measurements of the mean-squared displacements of single particles, we identified the transition to highly localized, immobile phases (i.e., immobile clusters and gels) with increasing polymer concentration. We quantified the microstructure of gels by means of the bond number distribution and number density fluctuations. Interestingly, the short-range microstructure was nearly identical between 5.1 and 13.4 mg/ml

samples, while the long-range structure exhibited a decrease of the structural heterogeneity, changing from "clusterlike" to "stringlike" structures with increasing polymer concentration. The dynamic and structural properties we obtained are consistent with observations by Dibble and co-workers [26]. Next, we observed the correlation between microscopic structure and mechanics of a colloidal gel by inducing and characterizing a local perturbation of the network. The sample at $C_p=2.0$ mg/ml shows dynamical (arrest) and structural characteristics (percolation) of a gel, as identified by Dibble and co-workers [26]. Despite this, however, the micromechanical response is not fully developed and the microstructure is extremely weak and unable to transmit microscopic stresses elastically. In contrast, in systems with stronger attractive interactions, particles in the gel microstructure move in the response of the probe particle with a strain, consistent with an elastic medium. Nonetheless, the clusterlike structures at $C_p=5.1$ and 10.0 mg/ml exhibit anomalous average strain fields, while the stringlike structure at $C_p=13.4$ mg/ml is consistent with the expected trend to length scales on the order of the gel particle dimensions. Rescaling the probe size used in the elastic medium model provided an estimate for the cluster sizes in the gel network. Consequently, this length scale correlated with structural differences (i.e., "clusterlike" and "stringlike") and identifies a different mechanical correlation length.

ACKNOWLEDGMENTS

The authors thank M. Solomon for his PMMA synthesis expertise and helpful comments, in addition to discussions with P. Spicer, J. Vermant, D. Vlassopoulos, N. Wagner, and E. Weeks. This research was supported by the National Science Foundation under Grant No. CBET-0238689 and IFPRI.

[1] S. Ramakrishnan, Y.-L. Chen, K. S. Schweizer, and C. F. Zukoski, Phys. Rev. E **70**, 040401(R) (2004).
[2] S. A. Shah, Y.-L. Chen, S. Ramakrishnan, K. S. Schweizer, and C. F. Zukoski, J. Phys.: Condens. Matter **15**, 4751 (2003).
[3] S. Manley, J. M. Skotheim, L. Mahadevan, and D. A. Weitz, Phys. Rev. Lett. **94**, 218302 (2005).
[4] C. J. Rueb and C. F. Zukoski, J. Rheol. **41**, 197 (1997).
[5] R. Buscall, I. J. McGrown, P. D. A. Mills, R. F. Stewart, D. Sutton, L. R. White, and G. E. Yates, J. Non-Newtonian Fluid Mech. **24**, 183 (1987).
[6] V. Trappe and D. A. Weitz, Phys. Rev. Lett. **85**, 449 (2000).
[7] H. Wu and M. Morbidelli, Langmuir **17**, 1030 (2001).
[8] W. H. Shih, W. Y. Shih, S. I. Kim, J. Liu, and I. A. Aksay, Phys. Rev. A **42**, 4772 (1990).
[9] A. H. Krall and D. A. Weitz, Phys. Rev. Lett. **80**, 778 (1998).
[10] R. Wessel and R. C. Ball Phys, Phys. Rev. A **46**, R3008 (1992).
[11] W. Y. Shih, W. H. Shih, and I. A. Aksay, J. Am. Ceram. Soc. **82**, 616 (1999).
[12] E. M. Furst and J. P. Pantina, Phys. Rev. E **75**, 050402(R) (2007).
[13] H. M. Wyss, E. V. Tervoort, and L. J. Gauckler, J. Am. Ceram. Soc. **88**, 2337 (2005).
[14] G. M. Channell, K. T. Miller, and C. F. Zukoski, AIChE J. **46**, 72 (2000).
[15] S. A. Shah, Y.-L. Chen, K. S. Schweizer, and C. F. Zukoski, J. Chem. Phys. **119**, 8747 (2003).
[16] Y.-L. Chen and K. S. Schweizer, J. Chem. Phys. **120**, 7212 (2004).
[17] D. A. Weitz and M. Oliveria, Phys. Rev. Lett. **52**, 1433 (1984).
[18] P. Meakin, Phys. Rev. Lett. **51**, 1119 (1983).
[19] Y. Kantor and I. Webman, Phys. Rev. Lett. **52**, 1891 (1984).
[20] H. F. van Garderen, W. H. Dokter, T. P. M. Beelen, R. A. van Santen, E. Pantos, M. A. J. Michels, and P. A. J. Hilbers, J. Chem. Phys. **102**, 480 (1995).
[21] H. Boukari, J. S. Lin, and M. T. Harris, J. Colloid Interface Sci. **194**, 311 (1997).
[22] H. F. van Garderen, E. Pantos, W. H. Dokter, T. P. M. Beelen, and R. A. van Santen, Modell. Simul. Mater. Sci. Eng. **2**, 295 (1994).
[23] S. Ramakrishnan, V. Gopalakrishnan, and C. F. Zukoski, Langmuir **21**, 9917 (2005).
[24] P. Varadan and M. J. Solomon, Langmuir **19**, 509 (2003).
[25] S. Manley, H. M. Wyss, K. Miyazaki, J. C. Conrad, V. Trappe, L. J. Kaufman, D. R. Reichman, and D. A. Weitz, Phys. Rev. Lett. **95**, 238302 (2005).
[26] C. J. Dibble, M. Kogan, and M. J. Solomon, Phys. Rev. E **74**, 041403 (2006).
[27] P. G. De Gennes, Macromolecules **14**, 1637 (1981).
[28] G. Pouyet, J. Francois, J. Dayantis, and G. Weill, Macromolecules **13**, 176 (1980).
[29] S. Asakura and F. Oosawa, J. Polym. Sci. **33**, 183 (1958).
[30] R. Verma, J. C. Crocker, T. C. Lubensky, and A. G. Yodh, Phys. Rev. Lett. **81**, 4004 (1998).
[31] L. A. Hough and H. D. Ou-Yang, Phys. Rev. E **73**, 031802 (2006).
[32] L. A. Hough and H. D. Ou-Yang, J. Nanopart. Res. **1**, 495 (1999).
[33] A. Meyer, A. Marshall, B. G. Bush, and E. M. Furst, J. Rheol. **50**, 77 (2006).
[34] M. H. Lee and E. M. Furst, Phys. Rev. E **74**, 031401 (2006).
[35] J. C. Crocker and D. G. Grier, J. Colloid Interface Sci. **179**, 298 (1996).
[36] R. N. Bracewell, *The Fourier Transform and Its Applications* (McGraw-Hill, New York, 1986).
[37] P. Poulin, J. Bibette, and D. A. Weitz, Eur. Phys. J. B **7**, 277 (1999).
[38] P. Varadan and M. J. Solomon, Langmuir **19**, 509 (2003).
[39] S. Torquato, *Random Heterogeneous Materials: Microstructure and macroscopic properties* (Springer, New York, 2002).
[40] J. P. Hansen and I. R. McDonald, *Theory of Simple Liquids* (Academic Press, San Diego, 1990).
[41] N. Phan-Thien and S. T. Kim, *Microstructures in Elastic Media: Principles and Computational Methods* (Oxford University Press, Oxford, 1994).